Water Research 215 (2022) 118223

Contents lists available at ScienceDirect

Water Research

journal homepage: www.elsevier.com/locate/watres

A plant-wide model describing GHG emissions and nutrient recovery options for water resource recovery facilities

Borja Solís [a], Albert Guisasola [a,*], Xavier Flores-Alsina [b], Ulf Jeppsson [c], Juan Antonio Baeza [a]

[a] GENOCOV, Departament d'Enginyeria Química, Biològica i Ambiental, Escola d'Enginyeria, Universitat Autònoma de Barcelona, Cerdanyola del Vallès, 08193 Barcelona, Spain
[b] PROSYS Research Centre, Department of Chemical and Biochemical Engineering, Technical University of Denmark, Building 229, DK-2800 Kgs, Lyngby, Denmark
[c] Division of Industrial Electrical Engineering and Automation (IEA), Department of Biomedical Engineering, Lund University, Box 118, SE-221 00 Lund, Sweden

ARTICLE INFO

Keywords:
Benchmarking
Control strategies
EBPR
GHG emissions
BSM2

ABSTRACT

In this study, a plant-wide model describing the fate of C, N and P compounds, upgraded to account for (on-site/off-site) greenhouse gas (GHG) emissions, was implemented within the International Water Association (IWA) Benchmarking Simulation Model No. 2 (BSM2) framework. The proposed approach includes the main biological N_2O production pathways and mechanistically describes CO_2 (biogenic/non-biogenic) emissions in the activated sludge reactors as well as the biogas production (CO_2/CH_4) from the anaerobic digester. Indirect GHG emissions for power generation, chemical usage, effluent disposal and sludge storage and reuse are also included using static factors for CO_2, CH_4 and N_2O. Global and individual mass balances were quantified to investigate the fluxes of the different components. Novel strategies, such as the combination of different cascade controllers in the biological reactors and struvite precipitation in the sludge line, were proposed in order to obtain high plant performance as well as nutrient recovery and mitigation of the GHG emissions in a plant-wide context. The implemented control strategies led to an overall more sustainable and efficient plant performance in terms of better effluent quality, reduced operational cost and lower GHG emissions. The lowest N_2O and overall GHG emissions were achieved when ammonium and soluble nitrous oxide in the aerobic reactors were controlled and struvite was recovered in the reject water stream, achieving a reduction of 27% for N_2O and 9% for total GHG, compared to the open loop configuration.

1. Introduction

In recent years, the scarcity of natural resources and the concern about climate change have shifted the water sector paradigm. Therefore, wastewater treatment plants (WWTPs) are becoming water resource recovery facilities (WRRFs). This fact has promoted both the chemical and environmental engineering community and the water industry to widen the scope of these utilities. To better understand and to design these new facilities, plant-wide modelling tools have become essential (Jeppsson et al., 2013). Wastewater treatment modelling researchers have integrated the main unit operations of a WRRF (primary clarifier, biological reactor, secondary settler, thickeners, anaerobic digester, dewatering unit, etc.) to account for all the interactions amongst processes (Barat et al., 2013; Gernaey et al., 2014; Grau et al., 2007; Hauduc et al., 2019; Solon et al., 2017; Vaneeckhaute et al., 2018) in view of simulating WRRF under different scenarios and of designing novel control strategies for a better performance.

Plant-wide WRRF modelling comprises chemical and physico-chemical models to assess the new challenges of the wastewater treatment. Particularly, precipitation models of common chemical compounds in wastewater (Hauduc et al., 2015; Kazadi Mbamba et al., 2016, 2015b), aqueous phase chemistry models (Flores-Alsina et al., 2015; Solon et al., 2015) and mass transfer models (Amaral et al., 2019; Lizarralde et al., 2015) have been proposed and calibrated to study different subprocesses of a WWRF in addition to the traditional activated sludge models (ASM) based on biological processes (Batstone et al., 2002; Henze et al., 2015). Recently, Solon and co-workers (Solon et al., 2017) proposed a novel plant-wide model capable of predicting the fate of phosphorus (P) in both water and sludge lines as well as the interactions with sulphur (S) and iron (Fe) thanks to the implementation of comprehensive physico-chemical process models. This work combined a

* Corresponding author.
E-mail addresses: borja.solis@uab.cat (B. Solís), albert.guisasola@uab.cat (A. Guisasola), xfa@kt.dtu.dk (X. Flores-Alsina), ulf.jeppsson@iea.lth.se (U. Jeppsson), JuanAntonio.Baeza@uab.cat (J.A. Baeza).

https://doi.org/10.1016/j.watres.2022.118223
Received 8 September 2021; Received in revised form 20 January 2022; Accepted 23 February 2022
Available online 25 February 2022

Nomenclature

A^2/O	Anaerobic-Anoxic-Aerobic
ABAC	Aeration-based ammonium controller
AD	Anaerobic digester
ADM1	Anaerobic Digestion Model No. 1
AER	Aerobic section
ANAER	Anaerobic section
ANOX	Anoxic section
AOB	Ammonia Oxidizing Bacteria
AS	Activated Sludge
ASM	Activated Sludge Model
ASM2d	Activated Sludge Model No. 2d
BOD	Biological Oxygen Demand
BSM2	Benchmark Simulation Model No. 2
BSM2-PSFe	BSM2 for Phosphorus, Sulfur and Iron
BSM2G	BSM2 Greenhouse gas
C	Carbon
$Ca_3(PO_4)_2$	Amorphous calcium phosphate
$Ca_5(PO_4)_3OH$	Hydroxyapatite
$CaCO_3$	Calcite
CBIM	Continuity-based interfacing method
CH_4	Methane
CO_2	Carbon dioxide
CO_{2e}	Carbon dioxide equivalents
COD	Chemical Oxygen Demand
$CONV_{AS\text{-}AD}$	Conversion ASM-ADM interface
DEN pathway	Denitrification pathway
DEW	Dewatering unit
D_i	Diffusivity of component i in liquid phase ($m^2\ d^{-1}$)
DO	Dissolved Oxygen
D_{O2}	Diffusivity of oxygen in liquid phase ($m^2\ d^{-1}$)
EBPR	Enhanced Biological Phosphorus Removal
N_2O-EF	Nitrous Oxide Emission Factor (%)
$E_{production}$	Electricity production
EQI	Effluent Quality Index
FA	Free Ammonia
Fe	Iron
$FeCl_3$	Ferric Chloride
FeS	Iron Sulphide
FNA	Free Nitrous Acid
GHG	Greenhouse gas
GWP	Global Warming Potential
H_2	Hydrogen gas
H_2O	Water
H_2S	Hydrogen sulphide
HCO_3^-	Bicarbonate
HFO	Hydrous Ferric Oxides
IC	Inorganic Carbon
$K_{H,i}$	Henry's constant for the specie i
k_La_i	Mass transfer coefficient for component i (d^{-1})
k_La_{O2}	Mass transfer coefficient for oxygen (d^{-1})
KNH_4PO_4	k-Struvite
$Mg(OH)_2$	Magnesium Hydroxide
$MgCO_3$	Magnesite
$MgHPO_4$	Newberyite
$MgNH_4PO_4$	Struvite
MLSS	Mixed Liquor Suspended Solids
MMP	Multiple Mineral Precipitation
N	Nitrogen
N_2	Nitrogen gas
N_2O	Nitrous oxide
NaOH	Sodium hydroxide
ND pathway	Nitrifier Denitrification pathway
NH_2OH	Hydroxylamine
NN pathway	Nitrifier Nitrification pathway
NO	Nitric Oxide
NO_2^-	Nitrite
NO_3^-	Nitrate
NO_x	Oxidized forms of nitrogen
O_2	Oxygen gas
OCI	Operational Cost Index
OHO	Ordinary Heterotrophic Organism
P	Phosphorus
PAO	Polyphosphate Accumulating Organisms
PCM	Physico-Chemical Models
P_i	Partial pressure of the gas specie i
PI	Proportional Integral controller
P_{inorg}	Inorganic phosphorus
P_{org}	Organic phosphorus
PRIM	Primary clarifier
$PROCESS_{AS\text{-}AD}$	Process ASM-ADM interface
Q_w	Purge flow rate
S	Sulphur
S_A	Acetate (ASM) (gCOD m^{-3})
S_{aa}	Amino acids (ADM) (kgCOD m^{-3})
S_{ac}	Acetate (ADM) (kgCOD m^{-3})
SEC	Secondary settler
S_F	Soluble fermentable (ASM) (gCOD m^{-3})
S_{fa}	Fatty acids (ADM) (kgCOD m^{-3})
SI	Saturation index for mineral precipitation
S_I	Unbiodegradable soluble organics (ASM) (gCOD m^{-3})
S_{IC}	Inorganic Carbon (ASM, ADM) (kmol m^{-3})
S_{N2O}	Nitrous oxide (ASM) (gN m^{-3})
S_{NH2OH}	Hydroxylamine (ASM) (gN m^{-3})
S_{NH4}	Ammonium plus ammonia nitrogen (ASM) (gN m^{-3})
S_{NO}	Nitric oxide (ASM) (gN m^{-3})
S_{NO2}	Nitrite (ASM) (gN m^{-3})
S_{O2}	Dissolved oxygen (ASM) (gO m^{-3})
S_{PO4}	Phosphate (ASM) (gP m^{-3})
SRT	Sludge Retention Time
S_{su}	Sugars (ADM) (kgCOD m^{-3})
ST	Storage tank
T	Temperature
THK	Thickener
TIV	Time In Violation
TKN	Total Kjeldahl Nitrogen
TN	Total Nitrogen
TP	Total Phosphorus
TSS	Total Suspended Solids
VS	Volatile Solids
WRRF	Water Resource Recovery Facility
WWTP	Waste Water Treatment Plant
X_{AOB}	Ammonia Oxidizing Bacteria (ASM) (gCOD m^{-3})
X_{ch}	Carbohydrates (ADM) (kgCOD m^{-3})
X_i	Mineral concentration in solid phase (PCM) (kmol m^{-3})
X_I	Inert particulates organics (ASM, ADM) (gCOD m^{-3}) (kgCOD m^{-3})
X_{li}	Lipids (ADM) (kgCOD m^{-3})
X_{NOB}	Nitrite Oxidizing Bacteria (ASM) (gCOD m^{-3})
X_{PP}	Polyphosphates (ASM, ADM) (gP m^{-3}) (kgP m^{-3})
X_{pr}	Proteins (ADM) (kgCOD m^{-3})
X_S	Biodegradable particulate organics (ASM) (gCOD m^{-3})
X_{TSS}	Total Suspended Solids (ASM) (gTSS m^{-3})
REC	Recovery unit

modified Activated Sludge Model No. 2d (ASM2d) model with a speciation model routine to predict pH at each time step (Flores-Alsina et al., 2015). This model evaluated and compared several energy and nutrient recovery strategies, but without accounting for GHG emissions.

Indeed, GHG emissions should be included when evaluating the overall sustainability of control/operational strategies for water resource recovery to add another important criterion in the multivariable space of performance assessment; otherwise, a good a priori control structure providing excellent effluent quality and lower costs could obtain this at the expense of high GHG emissions that are not being considered. Previous modelling studies have already included GHG emissions as a potential performance criterion when evaluating the sustainability of WWTPs. amongst the GHGs, N_2O emissions, which have a 300-fold stronger global warming effect than carbon dioxide CO_2 (IPCC, 2013), have recently received a lot of attention. Several extensions based on ASM models have been proposed in the literature to better describe N_2O emissions during biological nitrogen removal (Domingo-Félez et al., 2017; Mannina et al., 2016; Massara et al., 2018; Ni and Yuan, 2015; Pocquet et al., 2016). However, although some parameters of the models are pH-dependent, the evolution of pH in the different reactors is not predicted since the effect on pH of the processes taking place are not considered. Specifically the growth rate of nitrifiers depends on pH, and consequently the N_2O emissions produced by nitrifiers cannot be described accurately for several operational conditions (Su et al., 2019). In addition, CO_2 emissions are typically not accounted for, since the evolution of inorganic carbon (IC) is not modelled. However, nitrifiers growth depends on IC availability (Guisasola et al., 2007; Torà et al., 2010; Wett and Rauch, 2003; Zhang et al., 2018) and its limitation could be significant in some scenarios.

One of the most used plant-wide model that takes into account the GHG emissions is the BSM2G (Flores-Alsina et al., 2011). Several works in the literature have applied this model to study the effect on GHG emissions when implementing different control/operational strategies (Barbu et al., 2017; Flores-Alsina et al., 2014, 2011; Santín et al., 2018, 2017; Sweetapple et al., 2015). However, BSM2G cannot describe the transformations and fate of P in the plant and, moreover, not all the known N_2O production pathways are included in this model. Indeed, N_2O could be produced during the denitrifying phosphorus removal process (Liu et al., 2015). Hence, a new model extension is needed to enable the evaluation of all the potential GHG emission sources when integrating the potential resource recovery mechanisms in WRRFs.

The current limitations of the previous approaches create the need to define a new extended benchmarking scenario (BSM2-PSFe-GHG) including biological COD/N/P removal, GHG emissions, and chemical and physico-chemical models to evaluate resource recovery in WRRFs. The main objective of the present work is to develop and evaluate this BSM2-PSFe-GHG plant-wide benchmarking scenario by integrating: i) the biological model ASM2d-N_2O proposed by Massara et al. (2018) accounting for both enhanced biological phosphorus removal (EBPR) and the most recently reported N_2O production pathways, ii) potential sources of GHG emissions through the WRRF (updated from Flores-Alsina et al. (2011)), iii) plant-wide modelling of detailed P chemical processes (Solon et al., 2017) and iv) development of novel control strategies based on nitrite and nitrous oxide sensors to mitigate N_2O emissions. Once the development of the BSM2-PSFe-GHG sub-models and their interfaces is detailed, simulations will help to understand how novel nutrient recovery/control strategies can affect GHG emissions in a plant-wide context. In this sense, this work aims at i) studying the effect on GHG emissions when implementing nutrient recovery/control strategies and ii) designing and implementing novel control/operational strategies to optimise plant performance while reducing the GHG emissions.

2. Material and methods

2.1. BSM2-PSFe-GHG description

2.1.1. Biological models

The ASM2d-PSFe-N_2O model defined in this work merges the BSM2-PSFe approach of Solon et al. (2017) and the ASM2d-N_2O model of Massara et al. (2018) that has been successfully applied to describe N_2O emissions in full-scale WWTPs (Solís et al., 2022). Hence, ASM2d-PSFe-N_2O describes simultaneous biological C, N and P removal, as well as the chemical and biological processes related to S and Fe and N_2O production and emission. Therefore, ASM2d-PSFe-N_2O presents five new state variables compared to the BSM2-PSFe model (i.e., S_{NO2}, S_{NO}, S_{N2O}, S_{NH2OH} and X_{NOB}). The N_2O biological pathways adapted from Massara et al. (2018) are:

1) NH_2OH oxidation pathway (NN pathway): N_2O is produced from the reduction of NO by the enzyme “Nor” of AOB coupled with the oxidation of NH_2OH to NO_2^- (Pocquet et al., 2016);
2) AOB nitrifier denitrification pathway (ND pathway): N_2O is produced from NO_2^- reduction to NO and subsequently to N_2O by AOB. These two processes are lumped in one single reaction as in Pocquet et al. (2016);
3) heterotrophic denitrification pathway (DEN pathway): N_2O is produced as an intermediate of the denitrification processes either by OHO or PAO (Hiatt and Grady, 2008).

The three biological N_2O production pathways were included in the ASM2d-PSFe-N_2O model to account for all the known biological N_2O production pathways and to fairly assess the contribution of each pathway under dynamic conditions and under the different control/operational strategies implemented. The stoichiometric matrix and the continuity verification of the modified ASM2d-PSFe-N_2O model were calculated as in Hauduc et al. (2010) and are provided in the Supplementary Information Section.

The anaerobic digestion model (ADM) implemented is an extension of the ADM1 model (Batstone et al., 2002), reproducing the biological and chemical interactions between P, S and Fe as reported in previous works (Flores-Alsina et al., 2016; Solon et al., 2017). The kinetic parameters of both models can be obtained from the software implementation or from the original sub-models (Flores-Alsina et al., 2016; Massara et al., 2018; Solon et al., 2017).

2.1.2. Physico-chemical models (PCMs)

BSM2-PSFe-GHG embraces three different PCMs as proposed in the BSM2-PSFe approach (Solon et al., 2017): the pH and ion speciation/pairing model (aqueous phase chemistry model), the multiple mineral precipitation (MMP) model and the gas-liquid mass transfer model.

2.1.2.1. pH and ion speciation/pairing. A general aqueous phase chemistry model is used in both ASM and ADM, describing the pH variation and ion pairing at each time step (Flores-Alsina et al., 2015; Solon et al., 2015). The aqueous phase chemistry model corrects for ionic strength via the Davies' approach for chemical activity (Solon et al., 2017). The acid-base parameters and the activity coefficients are temperature-dependent and all calculations are performed under non-ideal conditions. The acid-base equilibria are described as a set of implicit algebraic equations and solved at each integration step of the ordinary differential equation solver. The species concentrations take part in the biological and physico-chemical processes. A more detailed description of the aqueous phase chemistry model can be found in Flores-Alsina et al. (2015) and Solon et al. (2015).

The integration of the pH and ion speciation allows to account for weak acid-base conditions within the N_2O production processes, since the growth rates of nitrifiers (X_{AOB} and X_{NOB}) are functions of their substrates, i.e. free ammonia (FA, NH_3) and free nitrous acid (FNA, HNO_2), respectively.

2.1.2.2. Multiple mineral precipitation (MMP). The precipitation equations are integrated as temperature dependent reversible processes with the saturation index (SI) as the chemical driving force (Stumm and Morgan, 1996). The SI was calculated by comparing the multiplication of the chemical activities of the dissolved ions of each mineral with its solubility product. For a given aqueous phase, three conditions can occur (Kazadi Mbamba et al., 2015a): i) SI < 0, the aqueous phase is undersaturated and the mineral is dissolved; ii) SI = 0, the aqueous phase is at equilibrium; or iii) SI > 0, the aqueous phase is oversaturated and chemical precipitation may occur. The precipitation rate depends on the kinetic rate coefficient, the species concentration, the mineral solid phase and the order of the reaction (Kazadi Mbamba et al., 2015a, 2015b; Solon et al., 2017). The MMP model includes the most likely minerals to precipitate during wastewater treatment: calcite ($CaCO_3$), hydroxyapatite ($Ca_5(PO_4)_3(OH)$), amorphous calcium phosphate ($Ca_3(PO_4)_2$), struvite ($MgNH_4PO_4.6H_20$), K-struvite ($MgKPO_4{\cdot}6H_20$), newberyite ($MgHPO_4{\cdot}3H_20$), magnesite ($MgCO_3$) and iron sulphide (FeS). The simplified approach of Hauduc et al. (2015) is implemented to describe the precipitation of hydrous ferric oxides (HFOs), the phosphate adsorption and phosphate co-precipitation to better estimate the phosphorus chemical precipitation.

2.1.2.3. Gas-liquid transfer. The gas-liquid transfer processes are described for the gas components: CO_2, O_2, NO, N_2O, N_2 and H_2S. The gas-liquid transfer is based on Fick's first law (Eq. (1)), which states that the transfer rate (ρ_i) is proportional to the global mass transfer coefficient ($k_L a_i$) and the driving force is the difference between the saturation concentration and the concentration of the gas in the liquid phase. The saturation concentration is calculated through Henry's law, which states that there is a proportionality ($K_{H,i}$) between the saturation concentration of the gas dissolved in the liquid and the partial pressure of the gas (P_i):

$$\rho_i = k_L a_i \cdot (K_{H,i} \cdot P_i - C_i) \tag{1}$$

The mass transfer coefficient for each gas (i = CO_2, O_2, NO, N_2O, N_2 and H_2S) is calculated from Eq. (2) as the square root of the ratio of the diffusivities of the gaseous component in the liquid (D_i) to that of oxygen (D_{O2}) and proportional to the mass transfer coefficient of the reference compound oxygen (Lizarralde et al., 2015):

$$k_L a_i = k_L a_{o_2} \cdot \left(\frac{D_i}{D_{o_2}}\right)^{1/2} \tag{2}$$

The gas-liquid transfer processes in ADM are included for the following gas components: H_2O, CO_2, H_2, CH_4 and H_2S, and are implemented as described by Batstone et al. (2002).

2.2. Model integration

The different sub-models ($ASM2d\text{-}PSFe\text{-}N_2O$, ADM and PCMs) in BSM2-PSFe-GHG were integrated using model interfaces. The ASM→ADM and ADM→ASM interfaces are based on the continuity-based interfacing method (Nopens et al., 2009) to ensure elemental mass and charge conservation. The interfaces consider instantaneous processes (i.e. $PROCESS_{AS\text{-}AD}$) and state variable conversions (i.e. $CONV_{AS\text{-}AD}$). The ASM→ADM interface $PROCESS_{AS\text{-}AD}$ involves: (1) the removal of COD demanding compounds (NH_2OH, O_2, NO_3^-, NO_2^- NO and N_2O) with the associated growth of biomass, and (2) the decay of biomass (OHO, PAO, AOB and NOB) to produce proteins (X_{pr}), lipids (X_{li}), carbohydrates (X_{ch}) and inert particulate organics (X_I). The $CONV_{AS\text{-}AD}$ involve (1) the conversion of soluble fermentable organics (S_F) to amino acids (S_{aa}), sugars (S_{su}) and fatty acids (S_{fa}); (2) the conversion of biodegradable particulate organics (X_S) to X_{pr}, X_{li} and X_{ch}; and (3) the direct mapping of acetate (S_A to S_{ac}) and inert soluble and particulate organics (S_I and X_I) (Solon et al., 2017). Regarding the ADM→ASM interface, a comprehensive description of the involved processes and conversion can be found in Flores-Alsina et al. (2016). Finally, the PCMs integration into ASM and ADM models was made following the procedures detailed in the original works (Flores-Alsina et al., 2015; Solon et al., 2017, 2015).

2.3. Plant layout and ancillary processes

BSM2-PSFe-GHG was implemented in the same plant layout as the BSM2-PSFe (Solon et al., 2017). The WRRF consists of a primary clarifier (PRIM), an activated sludge section (AS), a secondary clarifier (SEC), a sludge thickener (THK), an anaerobic digester (AD), a dewatering unit (DEW) and finally a storage tank (ST) (Fig. 1). Additional models were considered to simulate the ancillary processes PRIM, SEC, THK, DEW and ST. The PRIM (900 m^3) was modelled according to Otterpohl and Freund (1992) with different settling velocities for biodegradable and non-biodegradable compounds (Wentzel et al., 2006). The AS had an A^2/O configuration consisting of 7 tanks in series: Tanks 1 and 2 were anaerobic (ANAER1 and ANAER2) with a total volume of 2000 m^3; tanks 3 and 4 were anoxic (ANOX1 and ANOX2) with a total volume of 3000 m^3 while tanks 5, 6 and 7 were aerobic (AER1, AER2 and AER3) with a total volume of 9000 m^3. The SEC (surface of 1500 m^2 and height of 4 m) was modelled according to the double exponential settling velocity function of Takács et al. (1991) in a ten-layer one-dimensional settler. The THK and DEW units were modelled as ideal units, with no biological activity and a constant percentage of TSS in the concentrated sludge flows. The AD had a working volume of 3400 m^3 and a headspace volume of 300 m^3. The ST was modelled as a non-reactive, ideally mixed tank of 160 m^3. Additional information about the plant design and default operational conditions can be found in Gernaey et al. (2014) and Solon et al. (2017).

The influent was generated following the principles proposed by Gernaey et al. (2011). Finally, the sensors and actuators were modelled with response time, delay and white noise to avoid creating unrealistic control applications (Rieger et al., 2003).

2.4. Estimation of GHG emissions

Different GHG compounds (CO_2, CH_4 and N_2O) type of emissions (biogenic and non-biogenic) and sources of emissions (direct or indirect) were accounted for in BSM2-PSFe-GHG. Estimates not explicitly calculated by the sub-models were estimated following the comprehensive methodology suggested by Flores-Alsina et al. (2014, 2011). The different sources of GHG emissions considered throughout the WRRF are:

- *Direct secondary treatment GHG emissions:* CO_2 generated from biomass respiration, CO_2 generated from BOD_5 oxidation, CO_2 credit from nitrification and N_2O generated during biological N-removal. CO_2 emissions are explicitly accounted for by $ASM2d\text{-}PSFe\text{-}N_2O$ and PCMs (i.e. pH and ion speciation/pairing and gas-liquid transfer models), by including IC instead of alkalinity as a state variable (Flores-Alsina et al., 2015). N_2O generated via the NN and ND pathways of AOB and DEN pathway of heterotrophic organisms (Massara et al., 2018).
- *Sludge processing GHG emissions*: GHG emissions during sludge processing are generated in the anaerobic digester. CO_2 and CH_4 emissions are explicitly calculated by the modified ADM1 model (Flores-Alsina et al., 2016; Solon et al., 2017). Fugitive emissions from AD and co-generation units are included as a total of 2.7% of the produced biogas that was slipped and un-combusted (Magnus Arnell, 2016). The remaining biogas is combusted in the gas-engine turbine and all the CH_4 is converted to CO_2, generating electricity

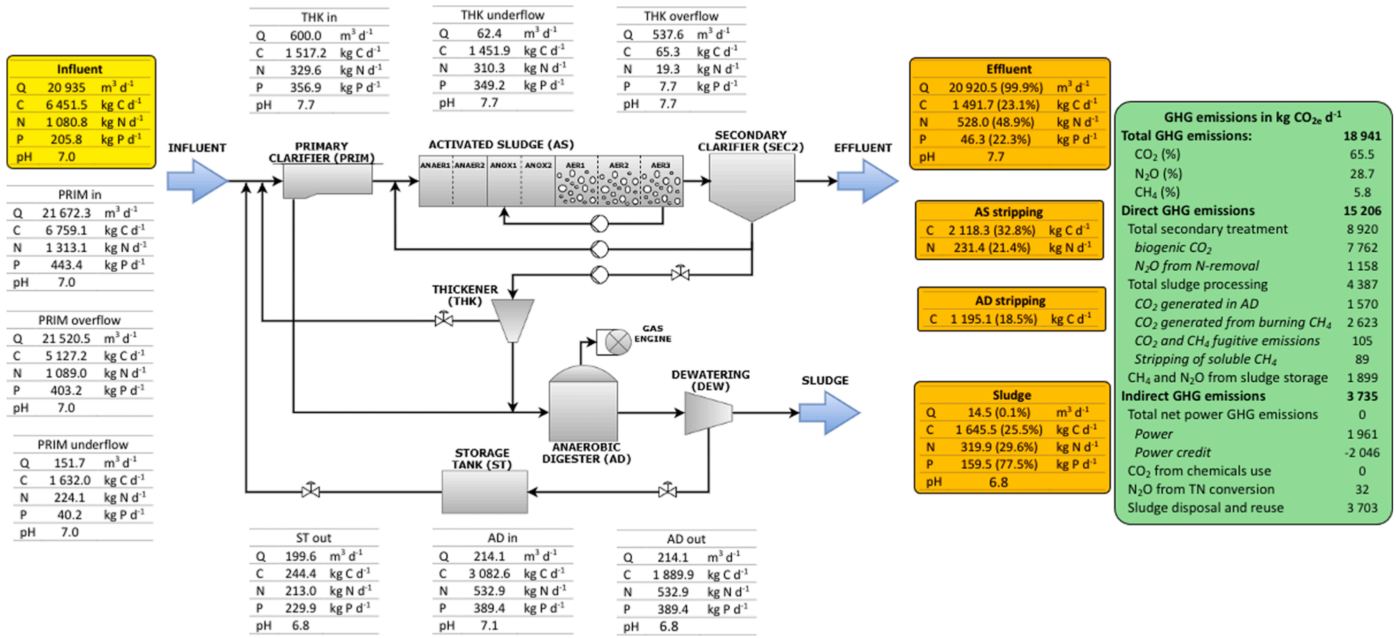

Fig. 1. Layout of the WRRF from the BSM2-PSFe-GHG. GHG emissions (green box) and overall and individual mass balances (C, N and P) and pH for the main streams of the WRRF are indicated in the tables (steady state results for A_0 open loop configuration). Inlet and outlet streams of the mass balances are highlighted in yellow and orange, respectively.

and heat. The CO_2 produced in the AD and the CO_2 produced in the combustion are released into the atmosphere. Finally, dissolved CH_4 (and H_2) in the digester effluent is assumed to be fully stripped in the following process units and emitted to the atmosphere. These emissions are accounted for in the AD (important to maintain mass balances). Potential N_2O emissions due to denitrification downstream of the AD unit (Oshita et al., 2014) were not considered since the DEW unit was modelled as a non-reactive unit. Moreover, it should be noted that neither NO_3^- nor NO_2^- were present in the AD.

- *Net power-related GHG emissions*: Net power is the difference between energy consumption and production. Energy production is the electricity produced by the AD turbine and it is calculated using a factor for the energy content of CH_4 (50 014 MJ (kg CH_4)$^{-1}$) and assuming an efficiency of 43% for electricity generation (Flores-Alsina et al., 2011). Energy consumption involves pumping, mixing, aeration and heating and is calculated using the operational cost index (OCI), see Section 2.5. A value of 0.359 kg CO_2 kWh^{-1} is selected for the CO_2 emission from net power production (European production mix) (IEA, 2011).
- *Embedded GHG emissions from chemicals use*: The possible addition of chemicals in the WRRF produces embedded indirect GHG emissions. The specific chemicals considered are: i) methanol dosage as external carbon source with a static factor of 1.54 kg CO_2 (kg methanol)$^{-1}$ (Flores-Alsina et al., 2011), ii) $FeCl_3$ for P precipitation, 0.16 kg CO_2 (kg $FeCl_3$)$^{-1}$, iii) NaOH to raise the pH, 1.24 kg CO_2 (kg NaOH)$^{-1}$ and iv) $Mg(OH)_2$ to favour the struvite precipitation, 1.17 kg CO_2 (kg Mg $(OH)_2$)$^{-1}$ (Gustavsson and Tumlin, 2013).
- *GHG emissions from effluent disposal:* N_2O is produced in the receiving effluent due to the partial conversion of the remaining TN. An emission factor of 5 g per kg TN discharged to recipient is obtained from the N_2O emissions corresponding to disposal in lakes and rivers (Arnell, 2016).
- *Sludge storage, disposal and reuse*: Direct emissions from sludge storage are estimated by assuming uncovered storage for 12 months as 8.68 kg CH_4 per ton of VS and 1.1% of TN in sludge emitted as N_2O (Arnell, 2016). After the sludge storage, it is transported for disposal and reuse, causing indirect emissions of CO_2, CH_4 and N_2O. The CO_2 emissions associated with the transport of biosolids are quantified by multiplying the truck movements by the distance of reuse. CO_2 emissions from mineralization are calculated based on the sludge mass multiplied by the carbon concentration and the conversion factor from C to CO_2. N_2O emissions are calculated based on a static factor of 0.01 kg N-N_2O per kg of TN. In total, three different sludge disposal alternatives are included: Agriculture (38% sludge disposal, 150 km from the WRRF), Compost (45% sludge, 20 km) and Forestry (17% sludge, 144 km) (Arnell, 2016; Bridle et al., 2008; Flores-Alsina et al., 2011).

Finally, all GHG emissions are converted into units of CO_2 equivalents (CO_{2e}) by the Global Warming Potentials (GWP). The GWP for a 100-year time horizon for N_2O and CH_4 are 298 kg CO_{2e} per kg N_2O and 34 kg CO_{2e} per kg CH_4, respectively (IPCC, 2013). Additional details on the implementation of GHG emissions can be found in Section 6.

2.5. Evaluation criteria

Three performance indices were used to assess the plant performance for the different control/operational strategies. Besides the classical evaluation criteria based on the effluent quality index (EQI) and the OCI (Gernaey et al., 2014; Nopens et al., 2010), total GHG emissions (in CO_{2e}) were added as an additional criterion, as first proposed by Flores-Alsina et al. (2014). This value enables the understanding of the synergies and trade-offs that different nutrient recovery control strategies can have on overall GHG emissions. On the other hand, EQI (kg pollution units d^{-1}) represents the overall pollution leaving the plant and is calculated with Eq. (3) as a weighted sum of effluent TSS, COD, BOD, TKN, NO_x (oxidized forms of nitrogen, including NO_3^-, NO_2^-, NO, N_2O and NH_2OH) and organic and inorganic P (P_{org} and P_{inorg}, respectively) (Solon et al., 2017).

$$\mathrm{EQI} = \frac{1}{t_{obs}\,1000}\int_{t_{start}}^{t_{stop}} \left[\beta_{\mathrm{TSS}}\cdot\mathrm{TSS}(t) + \beta_{\mathrm{COD}}\cdot\mathrm{COD}(t) + \beta_{\mathrm{BOD}}\cdot\mathrm{BOD}(t) + \beta_{\mathrm{TKN}}\cdot\mathrm{TKN}(t) + \beta_{\mathrm{NO_x}}\cdot\mathrm{NO_x}(t) + \beta_{\mathrm{P_{org}}}\cdot\mathrm{P_{org}}(t) + \beta_{\mathrm{P_{inorg}}}\cdot\mathrm{P_{inorg}}(t)\right]\cdot\mathrm{Q_e}(t)\cdot dt \tag{3}$$

where t_{obs} is the total evaluation period, the β_i are weighting factors for the different pollutants to convert them into general pollution units

(Solon et al., 2017) and Q_e is the effluent flow rate in $m^3\ d^{-1}$.

The OCI is calculated with Eq. (4) as a weighted sum of the costs related to aeration, pumping, mixing and heating energy, external carbon source, sludge production disposal, chemicals as well as the potential benefits of methane production and nutrients recovered (e.g. struvite).

$$OCI = AE + PE + f_{SP}\cdot SP + f_{EC}\cdot EC + ME - f_{MP}\cdot MP + \max(0, HE - 7MP) + f_{MA}\cdot MA + f_{Mg}\cdot Mg - f_{S_{recovered}}\cdot S_{recovered} \tag{4}$$

where AE is aeration energy, PE is pumping energy, SP is sludge production, EC is external carbon addition, ME is mixing energy, MP is methane production, HE is required heating energy for the AD, MA is metal addition, Mg is magnesium addition and $S_{recovered}$ is struvite recovered. The f_i are weighting factors and are selected as in Gernaey et al. (2014) and Solon et al. (2017).

Finally, other legal criteria, such as the percentage of time the plant is in violation (TIV), i.e. when effluent concentrations are above discharge limits for selected nutrients in the effluent, were also used to evaluate the plant performance.

2.6. Control strategies

Table 1 summarises the individual controllers and control strategies combining different controllers that were applied in this work. Figures S1-S5 (Supplementary Information Section) show the schematics of the control loops implemented in each control strategy. The default scenario (A_0) is the open-loop configuration (Gernaey et al., 2014), thus the air flow rate supplied to the aerobic reactors (value of the mass transfer coefficient k_La) and the purge flow rate were kept constant. The performance of each implemented control strategy is evaluated by comparison with A_0 by means of the evaluation criteria indices. The control strategies A_1 to A_3 are based on the improvement of the water quality (reduction of EQI and TIV for N and P species) by optimizing the aeration strategy, the sludge age in winter or by including nutrient recovery. Finally, the control strategies A_4 and A_5 are mainly focused on reducing the GHG emissions while maintaining good effluent quality and low operating costs.

All dynamic simulations (609 days) are preceded by a steady state simulation (300 days) but only data generated during the last 364 days of dynamic simulations are used to evaluate the implemented control strategies. The sensors characteristics applied in the implemented control strategies are summarized in section S2.

3. Results

3.1. Steady-state simulations

Fig. 1 shows the total GHG emissions, combined with the fractionation of GHG emissions (on-plant and off-plant), and the overall and individual mass balances for C, N and P as well as the pH under steady-state conditions for the A_0 scenario. amongst the total GHG emissions, 65% consisted of CO_2 (of which 63% of the total CO_2 emissions was biogenic CO_2 emitted in the biotreatment), 29% of N_2O (21% of the total N_2O emitted was produced in the biotreatment section through N-removal) and 6% of CH_4. The low CH_4 emissions were due to all the produced CH_4 in the AD was burnt in the gas engine unit and, therefore, transformed to CO_2 and energy. Most of the GHG emissions were direct emissions (80%), i.e. produced in the WRRF. The predicted indirect GHG emissions were mainly produced due to sludge disposal and reuse, since the CO_2 emissions produced due to electricity production were mitigated from the electricity generated in the cogeneration unit of CH_4 and no imbedded GHG emissions from chemicals use were produced.

Regarding the fate of C, the inlet C ends up in three different forms: i) 51.3% is emitted as CO_2: 32.8% in the AS section as biogenic CO_2, due to the organic matter oxidation and biomass respiration and 18.5% as combustion and leakages of biogas in the AD (this represents 38.7% of the inlet C to the digester), ii) 23.1% is dissolved in the effluent mainly in the form of S_{IC} (80%) and S_I (13.4%) and iii) 25.5% is disposed of in the sludge as particulate organics and biomass.

In the case of N, the inlet N ends up in three different phases: i) 49% is discharged in the effluent mainly as S_{NO3} (31.4%) and dissolved S_{N2} (56.5%), ii) 21.4% ends up in the gas phase of the biological reactors, mainly as N_2, but with 1.0% of the inlet N as $N{=}N_2O$, which is within the ranges reported by Massara et al. (2017) and Ahn et al. (2010) who obtained values of 0–3.3% of N_2O emission in 12 different WWTPs, and iii) the remaining 29.6% of the inlet N is disposed in the sludge, mainly as biomass and entrapped in particulate organics. One important outcome of this A_0 operation is its feasibility to accomplish N-removal despite its lack of active control, since the values of TKN (2.8 g N m^{-3}) and TN (11.0 g N m^{-3}) in the effluent for A_0 are below the BSM discharge limits (TKN_{limit} = 4 g N m^{-3}, TN_{limit} = 18 g N m^{-3}). The analysis of this scenario also shows the important effects of some recycled streams, such as the overflows of the thickener and the dewatering unit, which increase the N influent load to the plant by 21.5%.

Regarding the P results, only 22.3% of the influent P leaves the plant through the water line, mainly as soluble orthophosphate S_{PO4} (43.6%) and X_{PP} (39.7%) that overflows in the secondary settler. The obtained effluent TP concentration is 2.37 g P m^{-3}, above the BSM discharge limit of TP_{limit} = 2.0 g P m^{-3}. The remaining 77.7% of inlet P remain in the

Table 1
Characteristics of the implemented controllers and control strategies.

Controller→	DO	NH_4^+	MLSS	PO_4^{3-}	Magnesium	Nitrite	N_2O
Characteristics↓							
Measured variable (s)	S_{O2} in AER2	S_{NH4} in AER2	X_{TSS} and T in AER3	S_{PO4} in AER3	Effluent S_{PO4} in REC unit	S_{NO2} in AER2	S_{N2O} in AER2
Controlled variable	S_{O2} in AER2	S_{NH4} in AER2	X_{TSS} in AER3	S_{PO4} in AER3	$X_{Mg(OH)2}$ in REC unit	S_{NO2} in AER2	S_{N2O} in AER2
Set-point	- gO m^{-3}	2 g N m^{-3}	3000 g m^{-3} (if T > 15 °C) 4000 g m^{-3} (if T < 15 °C)	1.0 g P m^{-3}	50 g P m^{-3}	0.5 g N m^{-3}	0.01 g N m^{-3}
Manipulated variable	k_La in AER1, 2 & 3	S_{O2} set-point in AER2	Q_w	Q_{FeCl3}	$Q_{Mg(OH)2}$	S_{O2} set-point in AER2	S_{O2} set-point in AER2
Control algorithm	PI	Cascaded PI	PI	PI	PI	Cascaded PI	Cascaded PI
Control strategy							
A_0							
A_1	X	X	X				
A_2	X	X	X	X			
A_3	X	X	X		X		
A_4	X	X	X		X	X	
A_5	X	X	X		X		X

waste sludge, pointing out the possibility of recovering P from the anaerobic digestate. Moreover, the recycles of the thickener overflows and the reject water, 7.7 and 229.9 kg P d^{-1}, respectively, increase the influent P load by 95%.

3.2. Dynamic simulations

The dynamic simulation results of the default A_0 scenario and the runs with implemented control strategies A_1-A_5 are summarized in Table 2. In the case of A_0, 22.5% of the total GHG emissions come from N_2O during biological N-removal, which represents a N_2O emission factor (N_2O-EF) of 2.10%. This emission factor could be reduced by analysing which biological pathways are producing most of the N_2O and, then, designing adequate mitigation strategies Table 2. also shows that the effluent obtained is acceptable in terms of effluent average concentrations during the evaluated period. However, the percentages of TIV for ammonium and P are high (35.3% and 40.5%, respectively) and thus, there is a niche for a performance improvement using control strategies. In the following sections, the results for each implemented control strategy (Table 1) are presented and discussed. The GHG emissions and the overall and individual mass balances (Q, C, N and P) and pH for the main streams of the WRRF for each control strategy are reported in sections S3 and S4 (Supplementary Information Section).

3.2.1. Control strategy A_1: Ammonium cascade & waste controller

The A_1 control strategy involves three controllers. The first two control loops include two controllers following a cascade configuration, currently known as aeration-based ammonium controller (ABAC). In this configuration, the DO controller of the secondary feedback control loop is in charge of maintaining the DO concentration in AER2 by manipulating the aeration flow (k_La value), while the primary feedback control loop manipulates the DO set-point in AER2 using the ammonium concentration in AER2 as the controlled variable. The ammonium set-point in AER2 reactor is fixed at 2 g N m^{-3}. An additional control loop acts on the purge flow (Q_w) to maintain the desired X_{TSS} concentration in AER3. The X_{TSS} set-point depends on the temperature (Table 1). The X_{TSS} concentration is increased from 3 000 to 4 000 g TSS m^{-3} during winter conditions (i.e. $T < 15$ °C) to establish a longer sludge retention time (SRT) and to maintain the nitrification capacity (Solon et al., 2017; Vanrolleghem et al., 2010).

Table 2 shows that there is a reduction in N_2O emissions due to the increase of the DO-setpoint, which decreases the nitrite concentration compared to A_0 and leads to a reduction of N_2O emissions through the ND pathway Fig. 2.a shows that there are two different trends in N_2O emission rates depending on the season. On the one hand, the aeration demand is low during summer (day 254 to 357 and day 549 to 609), the DO ranges between 1 and 2 g O_2 m^{-3} and nitrite is accumulating in the reactors (Fig. 2g). This causes N_2O emissions via the ND pathway of AOBs to increase (Fig. 2d). On the other hand, during winter conditions, aeration increases and nitrite levels decrease, which deactivates the ND pathway. However, the production of N_2O by the NN and DEN pathways increases because the cascade NH_4^+ control has difficulty in maintaining the desired NH_4^+ concentration during winter (see Figs. 2d and 2g) considering the applied constraints in the DO set-point to avoid unrealistic control applications (minimum of 0 g O_2 m^{-3} and maximum of 6 g O_2 m^{-3}). The GHG emissions from the biotreatment (CO_2 biogenic plus N_2O from N-removal) and the total GHG emissions decreased (4.0% and 3.6%, respectively), due to the decrease in N_2O emissions. The variation of the waste flow rates during summer and winter led to an improvement in the AD performance, since more methane was produced ($E_{production}$ increased), which however led to an increase in AD emissions due to increased combustion of biogas.

EQI improved in A_1 due to lower effluent N concentrations: TKN decreased from 5.8 to 3.6 g N m^{-3} (A_0 vs A_1) and the TIV of ammonium decreased from 35.3 to 0.2%. The average P concentration remained the same and the total P concentration in the effluent decreased by only 0.1 g P m^{-3} compared to A_0. The OCI increased compared to A_0 mainly due to increased aeration costs during the winter period (i.e. when the temperature is below 15 °C, between days 357 and 549 of the simulation), since a higher DO set-point is required to maintain the desired ammonium concentration (Fig. 2g).

3.2.2. Control strategy A_2: Fe chemical precipitation of PO_4^{3-}

Control strategy A_2 aims at reducing the effluent P concentration via its chemical precipitation with Fe by adsorption and co-precipitation of phosphate species onto HFOs. A_2 includes A_1 and a PI controller that

Table 2
Performance evaluation criteria for each control strategy.

Control strategy →	A_0	A_1	A_2	A_3	A_4	A_5	**units**
Emitted CO_2 biogenic	7 467	7 510	7 616	7 470	7 569	7 527	kg CO_{2e} d^{-1}
Emitted N_2O N-removal	5 237	4 681	4 685	4 312	3 987	3 832	kg CO_{2e} d^{-1}
N_2O-EF total	2.10	1.33	1.35	1.27	1.17	1.11	%
Total emissions biotreatment	12 703	12 191	12 301	11 782	11 556	11 359	kg CO_{2e} d^{-1}
AD emissions	4 366	4 462	4 528	4 252	4 238	4 261	kg CO_{2e} d^{-1}
Total GHG emissions	**23 339**	**22 494**	**22 844**	**22 363**	**21 333**	**21 164**	**kg CO_{2e} d^{-1}**
Direct GHG emissions	18 970	18 582	18 796	17 743	17 491	17 326	kg CO_{2e} d^{-1}
Indirect GHG emissions	4 369	3 912	4 049	4 620	3 842	3 837	kg CO_{2e} d^{-1}
$N_{kjeldahl}$	5.8	3.6	3.5	3.8	3.6	3.6	g N m^{-3}
N_{total}	13.0	11.3	11.4	10.6	10.9	10.9	g N m^{-3}
P_{inorg}	1.0	1.0	0.5	0.1	0.1	0.1	g P m^{-3}
P_{total}	2.5	2.4	1.8	0.9	0.9	0.9	g P m^{-3}
TIV S_{NH4} (= 4 g N m^{-3})	35.3	0.2	0.6	0.2	0.1	0.1	%
TIV N_{total} (= 18 g N m^{-3})	0.2	0.0	0.0	0.0	0.0	0.0	%
TIV P_{total} (= 2 g P m^{-3})	40.5	34.1	20.0	0.3	0.3	0.3	%
EQI	**11 769**	**10 338**	**9 074**	**7 129**	**7 240**	**7 238**	**kg p.u. d^{-1}**
$E_{aeration}$	4 000	4 445	4 838	4 031	4 126	4 237	kWh d^{-1}
$E_{production}$ [a]	5 674	5 791	5 897	5 906	5 829	5 860	kWh d^{-1}
$SP_{disposal}$	4 033	4 068	4 532	3 643	3 632	3 641	kg TSS d^{-1}
Q_{FeCl3} [b]	0	0	88	0	0	0	kg Fe d^{-1}
$Q_{Mg(OH)2}$ [b]	0	0	0	80	80	80	kg Mg d^{-1}
$S_{recovered}$ [c]	0	0	0	442	442	442	kg struv d^{-1}
OCI	**11 864**	**12 306**	**16 109**	**10 045**	**10 224**	**10 362**	**–**

[a] Energy production. The electricity generated by the turbine, calculated as the energy content of methane gas.
[b] Relative costs for $FeCl_3$, $Mg(OH)_2$ and recovered struvite are the same as in Solon et al. (2017).
[c] $S_{recovered}$ refers to recovered struvite.

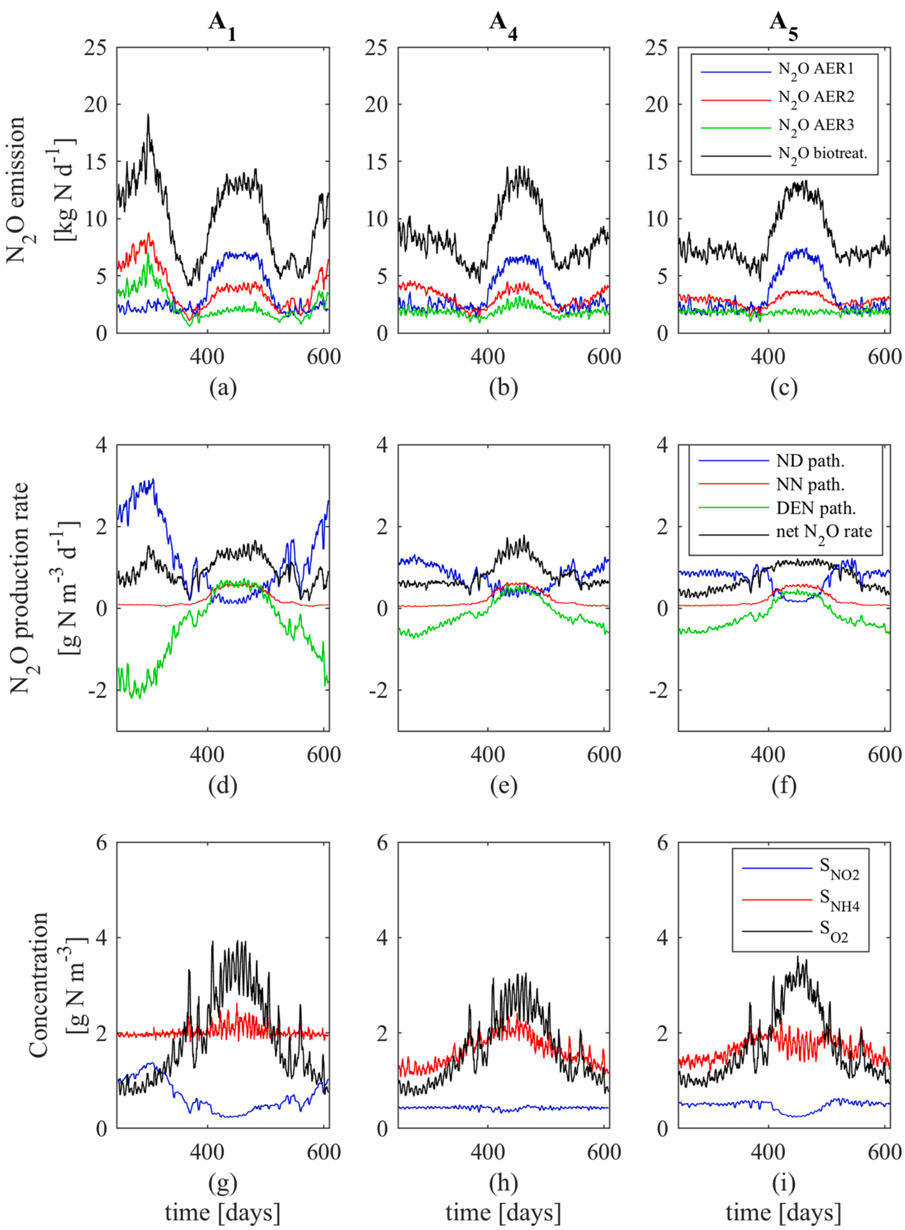

Fig. 2. Dynamic profiles of control strategies A_1 (a, d, g), A_4 (b, e, h) and A_5 (c, f, i). (a, b, c): N_2O emissions in the AS unit; (d, e, f): N_2O production rates in AER2 reactor and (g, h, i): nitrite, ammonium and DO concentrations in AER2 reactor. A 3-day first-order exponential filter is used to improve visualization of the results. Negative values of the DEN pathway mean that, for the 4-step denitrification process, the rate of N_2O reduction to N_2 is higher than that of N_2O production from NO. Additional dynamic profiles for all the control strategies are shown in section S4 of SI.

regulates the $FeCl_3$ addition in AER3 reactor to maintain the P concentration in AER3 reactor at the desired set-point of 1 g P m^{-3} (Table 1). The average S_{PO4} concentration in scenario A_0 already was 1 g P·m^{-3}, but high P peaks were observed in the effluent. The objective of A_2 is mitigating these P peaks avoiding the high TIV = 40.5% observed.

Regarding GHG emissions, total emissions in A_2 increased slightly due to i) more biogenic CO_2 was emitted: PAO activity decreased because there was less phosphate in the anaerobic reactor, resulting in a higher fraction of COD removed by heterotrophic biomass; this biomass produces more inorganic carbon than PAO when removing COD, ii) higher production of biogas and therefore higher emissions from the AD: the iron species enhance primary clarification and more COD is redirected to the AD system and iii) indirect CO_2 emitted by the use of $FeCl_3$. The observed N_2O emissions were the same as in control strategy A_1 because the N fluxes were not affected by the addition of iron (see Table 2).

A_2 led to a lower concentration of P in the effluent and, consequently, the TIV of total P decreased from 40.5% with A_0 to 20.0% with A_2 and the EQI was reduced by about 23% (Table 2). The phosphate controller was able to reduce the S_{PO4} peaks in the AER3 reactor with the addition of Fe, compared to control strategy A_0 (Table 2). However, the controller was not able to maintain the S_{PO4} at the desired set-point. The average $FeCl_3$ flow rate throughout the evaluation period was 88 kg Fe/d, which led to a considerable increase of the operational cost, mainly due to the iron dosage (2400 \$ (Ton Fe)$^{-1}$, (Solon et al., 2017)).

3.2.3. *Control strategy A_3: Struvite recovery*

Control strategy A_3 complements A_1 by including P- (and N-) recovery as struvite in the digester supernatant. The layout of the WRRF was modified by including a recovery unit (REC) based on struvite precipitation (see Figure S3 in Supplementary Information Section). The REC unit includes a crystallizer to support struvite precipitation, a storage tank for magnesium hydroxide ($Mg(OH)_2$) and a dewatering unit (Kazadi Mbamba et al., 2016; Solon et al., 2017). A PI controller was added to control the effluent P from the recovery unit at a set-point of 50 g P m^{-3} by manipulating the $Mg(OH)_2$ flow rate ($Q_{Mg(OH)2}$).

GHG emissions from the whole WRRF decreased (Table 2). N_2O emissions decreased slightly because the influent N load to the AS unit decreased due to struvite crystallization in the reject water stream and, thus, P- and N-recovery as struvite also had a potential benefit on GHG emissions due to more diluted streams. The struvite recovered was 442 kg d^{-1}, which resulted in 99.8 kg P d^{-1} (48.5% of the total P influent load) and 45.0 kg N d^{-1} recovered (4.2% of the total N influent load), respectively. The reject water P load was reduced from 232.3 kg P d^{-1} (A_1) to 11.2 kg P d^{-1} (A_3), which resulted in a 95% reduction in the influent P load to the biological reactors.

Table 2 shows that the average effluent P concentrations in A_3 were lower than those in strategies A_0 to A_2: the WRRF was able to discharge P below the legal limits most of the time (TIV of 0.3%) and EQI decreased by a significant 31% with respect to A_1. Table 2 also shows that OCI decreased 18% compared to A_1, i.e. struvite recovery is techno-economically feasible considering only the operational costs associated with the addition of Mg and struvite revenues in a current market scenario. More struvite could be recovered by lowering the phosphate set-point of the controller, since there was still a surplus of 11.2 kg d^{-1} of inorganic P available to be precipitated as struvite (Fig. 3a). However, this would imply a higher cost of $Mg(OH)_2$ and with the selected setpoint it was enough to meet P discharge limits. Struvite can be precipitated in a wide range of pH (between 7 and 11) with an optimum pH range between 8.0 and 9.5. The addition of $Mg(OH)_2$ was enough to increase pH from 7.1 to 8.3 (Fig. 3b) favouring struvite precipitation without requiring an additional aeration unit for CO_2 stripping nor the addition of more alkalinity such as NaOH (Kazadi Mbamba et al., 2016; Solon et al., 2017). Further studies are required to assess the capital costs associated with struvite recovery and additional transport costs (these costs were not considered in the evaluation criteria).

3.2.4. *Control strategy A_4: Ammonium & nitrite cascade controllers and struvite recovery*

Control strategy A_4 aims at reducing GHG emissions with a particular emphasis on N_2O emissions derived from biological N-removal. A_4 extends A_3 with a cascade PI nitrite controller in AER2 reactor. Nitrite concentration was maintained at the desired set-point by manipulating the set-point of the DO controller in conjunction with the ammonium cascade PI controller. Both controllers calculated an adequate DO set-point and the maximum value was chosen (see Table 1 for the characteristics of the controllers). The set-point signal of both controllers was smoothened using a first-order exponential filter with a time constant of 15 min to avoid numerical instabilities during solver integration.

A_4 led to the minimum GHG emissions with respect to the previously implemented strategies (A_0 to A_3): the N_2O emissions were reduced by 7.5% compared to A_3. The implementation of the nitrite PI cascade controller reduced the N_2O emissions during the summer conditions compared to A_1 (Figs. 2a and 2b), since one of the substrates of the ND pathway, i.e. nitrite, was minimized (Figs. 2d and 2e). The N_2O emissions during winter conditions remained the same as in A_1 because the ammonium PI cascade was preferentially fixing the DO set-point. The nitrification capacity should be increased in order to further reduce the N_2O emissions during winter by, for example, increasing the DO levels or the MLSS concentration, with the trade-off of further increasing the operational costs.

A_4 slightly increased the effluent N concentration in comparison to A_3 (2.8% increase in total N compared to A_3) due to more ammonium being nitrified in A_4 compared to A_3 (effluent TKN decreased by 5%) and the increase of effluent nitrate concentration. In this sense, the implementation of ammonium and nitrite cascade controllers also slightly increased OCI by 1.8%, compared to A_3, since the applied DO set-point was always the maximum of the ammonium and nitrite controllers and the aeration costs incremented by 2.3% compared to A_3. The same amount of struvite was obtained as in A_3 because the fluxes of P in the sludge line remained unaffected. Fig. 2h shows that during summer conditions (i.e. T above 15 °C) the DO set-point is mostly defined by the nitrite controller (NH_4^+ is below the set-point of 2 g N m^{-3} and NO_2^- concentration is around the set-point of 0.5 g N m^{-3}). The NH_4^+ controller is only activated during the daily peaks when the influent N load is high (in summer the DO set-point is defined by the NH_4^+ controller only 23% of the time). On the other hand, during winter conditions the DO set-point is defined most of the time (62%) by the NH_4^+ controller to ensure complete nitrification.

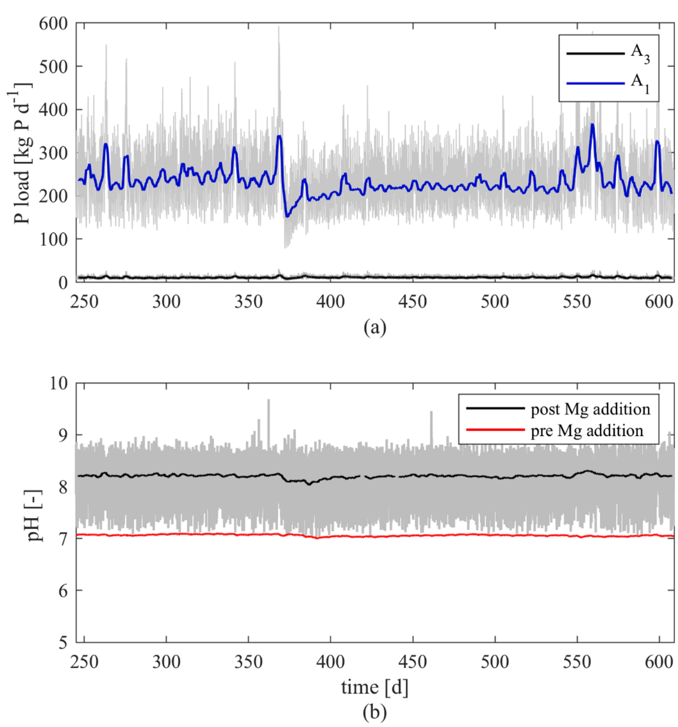

Fig. 3. a) Total P effluent load of the recovery unit (returns to water line) for control strategies A_1 and A_3. b) Simulated pH values of the recovery unit influent prior and post magnesium addition for control strategy A_3. A 3-day first-order exponential filter is used to improve the visualization of the results. Raw data is shown in grey.

3.2.5. *Control strategy A_5: Ammonium & nitrous oxide cascade controllers and struvite recovery*

A_5 is a modification of A_4 that also aimed at reducing N_2O emissions. New sensors have appeared in the market that enable the monitoring of soluble N_2O concentration in the reactors with high accuracy and, thus, allow designing novel mitigation strategies. For this reason, A_5 included a cascade PI controller based on the measurement and control of N_2O concentration in AER2. In a similar way to A_4, N_2O and NH_4^+ controllers calculated S_{O2} set-points for the DO controller and the chosen value was the maximum (Table 1).

The GHG emissions obtained were the lowest amongst all the control

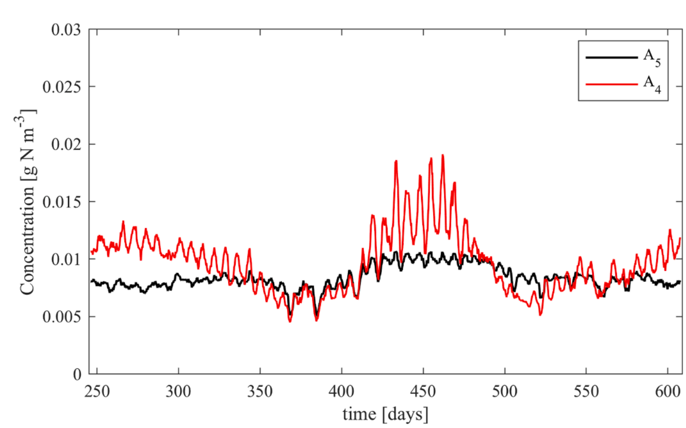

Fig. 4. Simulated soluble N_2O concentration in AER2 for A_4 and A_5. A 3-day first-order exponential filter is used to improve the visualization of the results.

strategies implemented (Table 2), with 13% reduction in N_2O emissions compared to A_1, and 1% reduction compared to A_4. Fig. 4 shows the concentration of soluble N_2O in AER2 predicted in A_4 and A_5. N_2O concentration in A_5 was much more constant due to the N_2O PI cascade controller, which actively imposed the DO set-point when the N_2O concentration in AER2 was too high. Only in the transition period from summer to winter (T around 15 °C), the cascade PI controllers of A_4 achieved lower N_2O concentrations (and lower N_2O emissions) than in A_5. This was due to the N_2O PI of A_5 being deactivated and the DO setpoint was being fixed by the NH_4^+ controller. On the other hand, during summer and winter, i.e. T above ~16 °C and T below ~14 °C, the cascade controllers of A_5 achieved lower N_2O soluble concentration in AER2 (Fig. 4) and lower global N_2O emissions (Fig. 2b and c). These results also point to a simpler alternative strategy that could lead to reduction in N_2O and GHG emissions. Reducing the NH_4^+ set-point in strategy A_1 or implementing a properly selected temperature-dependent NH_4^+ set-point (similar to the TSS controller) would probably provide some further improvements, although the automated set-point selection of the closed-loop control would be lost in this case.

The effluent concentrations and the TIV obtained for A_5 were the same as for A_4, therefore, a high effluent quality was obtained. However, the OCI was 1.3% higher than A_4, since slightly more oxygen was required to maintain the N_2O set-point: the DO set-point was set by the N_2O cascade PI in A_5 58% of the time whereas the DO set-point was fixed by the nitrite controller in A_4 56% of the time.

3.2.6. *Comparison of the evaluation criteria for the control strategies implemented*

Fig. 5 compares EQI, OCI, biogenic N_2O emissions and total GHG emissions for each control strategy implemented. The data are normalised considering 100% for the values obtained with the reference operation A_0. All control strategies led to a more sustainable overall plant performance, since all of them obtained a better effluent quality (i.e. lower EQI) and lower GHG emissions compared to the default scenario. Regarding operational costs, the ammonium cascade controller (A_1) increased the OCI by 4% compared to A_0 due to the more intense aeration demands. The chemical P precipitation strategy (A_2) increased the OCI by 36% compared to A_0 due to the high cost of $FeCl_3$ dosage. On the other hand, struvite precipitation in the reject water (control strategy A_3) was the most successful strategy in terms of EQI and OCI, leading to a reduction in EQI of 40% compared to A_0 and 31% compared to A_1, and a reduction in OCI of 11% and 14% compared to A_0 and A_1, respectively. These improvements were due to: 1) the potential benefits of struvite sales and 2) the reduction in influent load of P and N, which led to lower aeration demand. Control strategies A_4 and A_5 obtained higher reduction in N_2O emission from N-removal compared to A_0. Control strategies A_4 and A_5 merged the ammonium cascade controller of A_1 with another nitrite or soluble N_2O cascade controller and the struvite precipitation of A_3. Both control strategies led to higher operational costs than A_3, 1.8 and 2.8%, respectively, due to the increased aeration demand imposed by the cascade controllers. A_5 seems to have a better performance since it led to a reduction of the emitted N_2O in the biotreatment of 27% but at the expense of higher costs (i.e. 1.3% higher in A_5 compared to A_4). There is therefore a compromise between operational costs and GHG emissions, since operational costs increased slightly in both strategies compared to A_3, where the main difference between the objectives of A_3 compared to A_4 and A_5 was the reduction of GHG emissions, and moreover, A_4 and A_5 achieved the same EQI.

Finally, Fig. 5 shows that the largest reduction in total GHG emissions was 9% compared to A_0, despite the fact that the main aim of the novel control strategies is N_2O reduction. Other sources of GHG emissions were not reduced, such as indirect emissions (electricity, chemical usage, sludge storage and reuse) which represented about 20% of the total GHG emissions, and other direct GHG sources that were not controllable, such as biogenic CO_2 and methane combustion, which together represented around 50% of the total GHG emissions (see Table S1 of Supplementary Information Section).

4. Comparison with other works and limitations of the proposed methodology

The proposed BSM2-PSFe-GHG plant-wide model and the implemented control strategies results represent an improvement to the current BSM modelling framework BSM2-PSFe (Solon et al., 2017) by adding the GHG production and emission during nutrient removal and recovery operational/control strategies. In this sense, the BSM2-PSFe-GHG provides a new tool that shows, in a plant-wide context, the trade-offs that different novel control strategies had on the sustainability of the WRRF. On the other hand, the BSM2-PSFe-GHG updates previous works addressed to characterize GHG emissions, with a particular emphasis on N_2O emissions, which were designed for different plant-wide models (Flores-Alsina et al., 2014, 2011; Sweetapple et al., 2014) by: i) adding the GHG emissions to the most recent BSM modelling framework capable of simulating nutrient recovery strategies (Solon et al., 2017), ii) adding all the known biological N_2O pathways reported in the ASM2d-N_2O model (Massara et al., 2018), iii) improving the calculation of CO_2 emissions by including the general aqueous phase model (Flores-Alsina et al., 2015; Solon et al., 2017) and iv) updating the sources of direct and indirect GHG emissions (Flores-Alsina et al., 2011; Arnell, 2016).

The results reported for each control strategy were unified into three main groups (EQI, OCI and GHG) as proposed by Flores-Alsina et al.

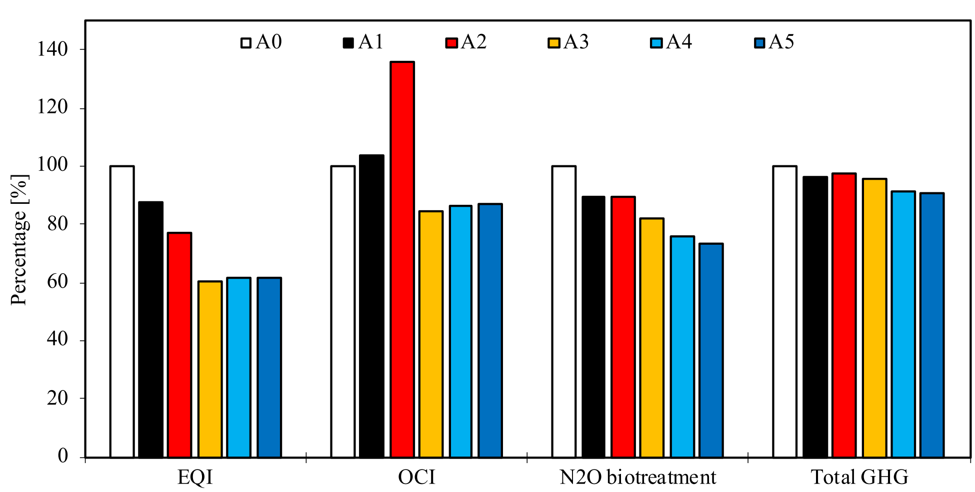

Fig. 5. Comparison of the evaluation criteria for the control strategies implemented. Data is shown in relative percentage compared to control strategy A_0.

(2014). This enabled a fairer evaluation of the different strategies, since none of the criteria depended on the others. Other works have proposed to unify the multicriteria into a single cost function by transforming effluent quality into monetary units by defining tariffs or taxes when the concentrations in the effluent are above a certain limit (Guerrero et al., 2012; Stare et al., 2007), or applying a defined weighted average of the different evaluation criteria (Machado et al., 2020). The benefits of the latter approach are that control strategies are compared with a single index. In this work, a unified cost function could be defined if GHG emissions were also translated into monetary units, by imposing tariffs due to high emissions. Special attention should be paid to defining the different weights of the cost function, since an optimisation of the cost function could lead to high GHG emissions or to poor effluent quality with low operational costs.

P recovery as struvite (strategies A_3 onwards) showed an improvement in the operational costs due to the potential revenues from struvite; however, these results should be taken with caution as the assumed price of struvite (200 \$ ton^{-1} as in Solon et al. (2017)) is very uncertain. In addition, struvite recovery improved effluent quality due to reduced P and N loading in the sludge line recycles and that also decreases operational costs. In fact, the OCI would also improve by 17.6%, compared to A_1, assuming no benefit from struvite sales. Finally, P recovery as struvite also showed a reduction in GHG emissions from the AS unit, mainly due to the decrease in the N influent load. Other important assumptions were made in the crystallizer unit model, such as ideal solids separation and simplified precipitate dissolution (Solon et al., 2017). In addition, potential pipe clogging in the REC unit due to struvite precipitation was not considered and is known to be a major issue during P recovery as struvite. These limitations in the crystallizer model should be addressed in future work to obtain a better estimation of struvite recovery.

One limitation of BSM2-PSFe-GHG is that capital expenditure was not included in the evaluation criteria and the comparison between control strategies was only subject to operational costs. Adding the capital costs of equipment, sensors, civil, electrical and piping will provide a more complete assessment (Machado et al., 2020; Ostace et al., 2013; Solon et al., 2017). For example, integrating P-recovery as struvite recovery implies a modification of the plant layout or adding a REC unit and all related equipment. That would result in a higher capital investment when retrofitting or upgrading the WRRF. On the other hand, P precipitation by Fe addition (control strategy A_2), showed higher operational costs than A_3 but this strategy "only" implies adding an extra dosing tank to the existing plant layout.

The proposed control strategies showed the logical steps that a WRRF manager should take to improve effluent quality (A_1 to A_3) and, afterwards, to reduce GHG emissions (A_4 and A_5). However, each of the control strategies could be optimized:

i) the location of the Fe addition in A_2 can be optimised to reduce operational costs as already reported (Kazadi Mbamba et al., 2019);
ii) each of the set-point values can be optimized as in Guerrero et al. (2011) in order to decrease the EQI and OCI, and to minimise GHG emissions. For instance, the reduction of the NH_4^+ set-point value from 2.0 to 1.0 g N m^{-3} in A_1 (Table 1) led to a 45% reduction in N_2O emissions, while the OCI increased by 4% and the EQI by 14%.
iii) N_2O emissions in the AS unit could be reduced by adding DO, NH_4^+, NO_2^- or N_2O sensors and controllers in each aerobic reactor to better control the WRRF as in Santín et al. (2017), who also aimed at reducing GHG emissions during wastewater treatment by using the BSM2G modelling framework (Flores-Alsina et al., 2011). This strategy enabled a more robust DO control and, therefore, a more robust control of N_2O emissions. However, the addition of multiple controllers in each aerobic reactor results in a more complex control structure for the biological reactors and would increase the capital and maintenance costs of the associated sensors, instruments and controllers.

5. Conclusions

In this paper, a novel plant-wide model that integrates the latest advances in energy and nutrient recovery modelling for an accurate description of N_2O- and EBPR-related processes is proposed. Five control strategies are evaluated in view of optimising plant performance, minimizing GHG emissions and implementing nutrient recovery. The main findings of the work are:

- Direct and indirect GHG emissions for CO_2, N_2O and CH_4 were quantified in the whole WRRF.
- Overall and individual mass balances quantify the distribution of C, N and P in the whole WRRF.
- All five control strategies led to an overall more efficient and sustainable plant performance.
- P-recovery as struvite led to decreased P and N concentrations in the biological reactors which reduced the N_2O emissions in the biotreatment by 17%, compared to the open loop configuration.
- The lowest N_2O and overall GHG emissions were achieved when ammonium and soluble nitrous oxide in the aerobic reactors were controlled, achieving a reduction of 24% and 27% for N_2O, respectively, and 9% for total GHG, compared to the open loop configuration.

Software availability

The MATLAB/SIMULINK code of the models presented in this work is available upon request. Using this code, readers will be able to reproduce the results included in this paper. To express interest, please contact with Dr. Juan Antonio Baeza (JuanAntonio.Baeza@uab.cat) or Dr. Albert Guisasola (Albert.Guisasola@uab.cat).

Declaration of competing interest

The authors declare that they have no known competing financial interests or personal relationships that could have appeared to influence the work reported in this paper.

Acknowledgements

The authors are very grateful to Dr Kimberly Solon (Ghent University, Belgium) for providing the BSM2-PSFe software code. Borja Solís is grateful for the PIF PhD grant funded by Universitat Autònoma de Barcelona. Borja Solís, Albert Guisasola and Juan Antonio Baeza are members of the GENOCOV research group (Grup de Recerca Consolidat de la Generalitat de Catalunya, 2017 SGR 1175, www.genocov.com). Xavier Flores-Alsina gratefully acknowledges the financial support provided by the Danish International Development Agency (Danida Fellowship center) in the frame of the ERASE project (grant number 18-M09-DTU) and the Danish MUDP (Miljøteknologisk udviklings- og demonstrationsprogram) under the project NACAT. A partial preliminary version of this paper was presented at Watermatex 2019 (Copenhagen, Denmark, September 2019).

Supplementary materials

Supplementary material associated with this article can be found, in the online version, at doi:10.1016/j.watres.2022.118223.

References

Ahn, J.H., Kim, S., Park, H., Rahm, B., Pagilla, K., 2010. N2O Emissions from activated sludge processes, 2008 - 2009 : results of a national monitoring survey in the United States. Environ. Sci. Technol. 44, 4505–4511. https://doi.org/10.1021/es903845y.

Amaral, A., Gillot, S., Garrido-Baserba, M., Filali, A., Karpinska, A.M., Plósz, B.G., De Groot, C., Bellandi, G., Nopens, I., Takács, I., Lizarralde, I., Jimenez, J.A., Fiat, J., Rieger, L., Arnell, M., Andersen, M., Jeppsson, U., Rehman, U., Fayolle, Y., Amerlinck, Y., Rosso, D., 2019. Modelling gas–liquid mass transfer in wastewater treatment: when current knowledge needs to encounter engineering practice and vice versa. Water Sci. Technol. 80, 607–619. https://doi.org/10.2166/wst.2019.253.

Arnell, M., 2016. Performance Assessment of Wastewater Treatment Plants. Lund University.

Barat, R., Serralta, J., Ruano, M.V., Jiménez, E., Ribes, J., Seco, A., Ferrer, J., 2013. Biological nutrient removal model no. 2 (BNRM2): a general model for wastewater treatment plants. Water Sci. Technol. 67, 1481–1489. https://doi.org/10.2166/wst.2013.004.

Barbu, M., Vilanova, R., Meneses, M., Santin, I., 2017. On the evaluation of the global impact of control strategies applied to wastewater treatment plants. J. Clean. Prod. 149, 396–405. https://doi.org/10.1016/j.jclepro.2017.02.018.

Batstone, D.J., Keller, J., Angelidaki, I., Kalyuzhnyi, S.V., Pavlostathis, S.G., Rozzi, A., Sanders, W.T.M., Siegrist, H., Vavilin, V.A., 2002. Anaerobic Digestion Model No. 1. IWA Sci. Tech. Rep. n.13. IWA Publ, London, UK.

Bridle, T., Shaw, A., Cooper, S., Yap, K.C., Third, K., 2008. Estimation of greenhouse gas emissions from wastewater treatment plants. In: Proceedings IWA Wordl Water Congress 2008, Vienna, Austria. September 7-12, 2008.

Domingo-Félez, C., Calderó-Pascual, M., Plósz, B.G., Smets, B.F., Sin, G., Plósz, B.G., 2017. Calibration of the comprehensive NDHA-N2O dynamics model for nitrifier-enriched biomass using targeted respirometric assays. Water Res. 126, 29–39. https://doi.org/10.1016/j.watres.2017.09.013.

Flores-Alsina, X., Arnell, M., Amerlinck, Y., Corominas, L., Gernaey, K.V., Guo, L., Lindblom, E., Nopens, I., Porro, J., Shaw, A., Snip, L., Vanrolleghem, P.A., Jeppsson, U., 2014. Balancing effluent quality, economic cost and greenhouse gas emissions during the evaluation of (plant-wide) control/operational strategies in WWTPs. Sci. Total Environ. 466–467, 616–624. https://doi.org/10.1016/j.scitotenv.2013.07.046.

Flores-Alsina, X., Corominas, L., Snip, L., Vanrolleghem, P.a, 2011. Including greenhouse gas emissions during benchmarking of wastewater treatment plant control strategies. Water Res. 45, 4700–4710. https://doi.org/10.1016/j.watres.2011.04.040.

Flores-Alsina, X., Kazadi Mbamba, C., Solon, K., Vrecko, D., Tait, S., Batstone, D.J., Jeppsson, U., Gernaey, K.V., 2015. A plant-wide aqueous phase chemistry module describing pH variations and ion speciation/pairing in wastewater treatment process models. Water Res. 85, 255–265. https://doi.org/10.1016/j.watres.2015.07.014.

Flores-Alsina, X., Solon, K., Kazadi Mbamba, C., Tait, S., Gernaey, K.V., Jeppsson, U., Batstone, D.J., 2016. Modelling phosphorus (P), sulfur (S) and iron (Fe) interactions for dynamic simulations of anaerobic digestion processes. Water Res. 95, 370–382. https://doi.org/10.1016/j.watres.2016.03.012.

Gernaey, K.V., Flores-Alsina, X., Rosen, C., Benedetti, L., Jeppsson, U., 2011. Dynamic influent pollutant disturbance scenario generation using a phenomenological modelling approach. Environ. Model. Softw. 26, 1255–1267. https://doi.org/10.1016/j.envsoft.2011.06.001.

Gernaey, K.V., Jeppsson, U., Vanrolleghem, P.A., Copp, J.B., 2014. Benchmarking of Control Strategies for Wastewater Treatment Plants. IWA Publishing. https://doi.org/10.2166/9781780401171.

Grau, P., de Gracia, M., Vanrolleghem, P.A., Ayesa, E., 2007. A new plant-wide modelling methodology for WWTPs. Water Res. 41, 4357–4372. https://doi.org/10.1016/j.watres.2007.06.019.

Guerrero, J., Guisasola, A., Comas, J., Rodríguez-Roda, I., Baeza, J.A., 2012. Multi-criteria selection of optimum WWTP control setpoints based on microbiology-related failures, effluent quality and operating costs. Chem. Eng. J. 188, 23–29. https://doi.org/10.1016/j.cej.2012.01.115.

Guerrero, J., Guisasola, A., Vilanova, R., Baeza, J.A., 2011. Improving the performance of a WWTP control system by model-based setpoint optimisation. Environ. Model. Softw. 26, 492–497. https://doi.org/10.1016/j.envsoft.2010.10.012.

Guisasola, A., Petzet, S., Baeza, J.A., Carrera, J., Lafuente, F.J., 2007. Inorganic carbon limitations on nitrification: experimental assessment and modelling. Water Res. 41, 277–286. https://doi.org/10.1016/j.watres.2006.10.030.

Gustavsson, D.J.I., Tumlin, S., 2013. Carbon footprints of Scandinavian wastewater treatment plants. Water Sci. Technol. 68, 887–893. https://doi.org/10.2166/wst.2013.318.

Hauduc, H., Rieger, L., Takács, I., Héduit, a, Vanrolleghem, P.A., Gillot, S., 2010. A systematic approach for model verification: application on seven published activated sludge models. Water Sci. Technol. 61, 825–839. https://doi.org/10.2166/wst.2010.898.

Hauduc, H., Takács, I., Smith, S., Szabo, A., Murthy, S., Daigger, G.T., Spérandio, M., 2015. A dynamic physicochemical model for chemical phosphorus removal. Water Res. 73, 157–170. https://doi.org/10.1016/j.watres.2014.12.053.

Hauduc, H., Wadhawan, T., Takács, I., Johnson, B., Bott, C., Ward, M., 2019. Incorporating sulfur reactions and interactions with iron and phosphorus into a general plant-wide model. Water Sci. Technol. 79, 26–34. https://doi.org/10.2166/wst.2018.482.

Henze, M., Gujer, W., Mino, T., van Loosedrecht, M., 2015. Activated Sludge Models ASM1, ASM2, ASM2d and ASM3. Water Intell. Online 5. https://doi.org/10.2166/9781780402369, 9781780402369–9781780402369.

Hiatt, W.C., Grady, C.P.L., 2008. An Updated Process Model for Carbon Oxidation, Nitrification, and Denitrification. Water Environ. Res. 80, 2145–2156. https://doi.org/10.2175/106143008X304776.

IEA, 2011. Emissions from Fuel combuistion. Highlights. Technical report. International Energy Agency, Paris, France n.d.

IPCC, 2013. Climate change 2013: the physical science basis. In: Contribution of Working Group I to the Fifth Assessment Report of the Intergovern - mental Panel on Climate Change. WGI [Stocker, T.F., D. Qin, G.-K. Plattner, M. Tignor, S.K. Allen, J. Boschung, A., n.d.

Jeppsson, U., Alex, J., Batstone, D.J., Benedetti, L., Comas, J., Copp, J.B., Corominas, L., Flores-Alsina, X., Gernaey, K.V., Nopens, I., Pons, M.-.N., Rodríguez-Roda, I., Rosen, C., Steyer, J.-.P., Vanrolleghem, P.A., Volcke, E.I.P., Vrecko, D., 2013. Benchmark simulation models, quo vadis? Water Sci. Technol. 68, 1–15. https://doi.org/10.2166/wst.2013.246.

Kazadi Mbamba, C., Batstone, D.J., Flores-Alsina, X., Tait, S., 2015a. A generalised chemical precipitation modelling approach in wastewater treatment applied to calcite. Water Res. 68, 342–353. https://doi.org/10.1016/j.watres.2014.10.011.

Kazadi Mbamba, C., Flores-Alsina, X., John Batstone, D., Tait, S., 2016. Validation of a plant-wide phosphorus modelling approach with minerals precipitation in a full-scale WWTP. Water Res. 100, 169–183. https://doi.org/10.1016/j.watres.2016.05.003.

Kazadi Mbamba, C., Lindblom, E., Flores-Alsina, X., Tait, S., Anderson, S., Saagi, R., Batstone, D.J., Gernaey, K.V., Jeppsson, U., 2019. Plant-wide model-based analysis of iron dosage strategies for chemical phosphorus removal in wastewater treatment systems. Water Res. 155, 12–25. https://doi.org/10.1016/j.watres.2019.01.048.

Kazadi Mbamba, C., Tait, S., Flores-Alsina, X., Batstone, D.J., 2015b. A systematic study of multiple minerals precipitation modelling in wastewater treatment. Water Res. 85, 359–370. https://doi.org/10.1016/j.watres.2015.08.041.

Liu, Y., Peng, L., Chen, X., Ni, B.J., 2015. Mathematical Modeling of Nitrous Oxide Production during Denitrifying Phosphorus Removal Process. Environ. Sci. Technol. 49, 8595–8601. https://doi.org/10.1021/acs.est.5b01650.

Lizarralde, I., Fernández-Arévalo, T., Brouckaert, C., Vanrolleghem, P., Ikumi, D.S., Ekama, G.A., Ayesa, E., Grau, P., 2015. A new general methodology for incorporating physico-chemical transformations into multi-phase wastewater treatment process models. Water Res. 74, 239–256. https://doi.org/10.1016/j.watres.2015.01.031.

Machado, V.C., Lafuente, J., Baeza, J.A., 2020. Systematic comparison framework for selecting the best retrofitting alternative for an existing water resource recovery facility. Water Environ. Res. 92, 2072–2085. https://doi.org/10.1002/wer.1368.

Magnus Arnell, 2016. Performance Assessment of Wastewater Treatment Plants. Multi-Objective Analysis Using Plant-Wide Models.

Mannina, G., Ekama, G., Caniani, D., Cosenza, A., Esposito, G., Gori, R., Garrido-Baserba, M., Rosso, D., Olsson, G., 2016. Greenhouse gases from wastewater treatment - a review of modelling tools. Sci. Total Environ. 551–552, 254–270. https://doi.org/10.1016/j.scitotenv.2016.01.163.

Massara, T.M., Malamis, S., Guisasola, A., Baeza, J.A., Noutsopoulos, C., Katsou, E., 2017. A review on nitrous oxide (N2O) emissions during biological nutrient removal from municipal wastewater and sludge reject water. Sci. Total Environ. 596–597. https://doi.org/10.1016/j.scitotenv.2017.03.191.

Massara, T.M., Solís, B., Guisasola, A., Katsou, E., Baeza, J.A., 2018. Development of an ASM2d-N2O model to describe nitrous oxide emissions in municipal WWTPs under dynamic conditions. Chem. Eng. J. 335, 185–196. https://doi.org/10.1016/j.cej.2017.10.119.

Ni, B.-.J., Yuan, Z., 2015. Recent advances in mathematical modeling of nitrous oxides emissions from wastewater treatment processes. Water Res. 87, 336–346. https://doi.org/10.1016/j.watres.2015.09.049.

Nopens, I., Batstone, D.J., Copp, J.B., Jeppsson, U., Volcke, E., Alex, J., Vanrolleghem, P.A., 2009. An ASM/ADM model interface for dynamic plant-wide simulation. Water Res. 43, 1913–1923. https://doi.org/10.1016/j.watres.2009.01.012.

Nopens, I., Benedetti, L., Jeppsson, U., Pons, M.N., Alex, J., Copp, J.B., Gernaey, K.V., Rosen, C., Steyer, J.P., Vanrolleghem, P.A., 2010. Benchmark Simulation Model No 2: finalisation of plant layout and default control strategy. Water Sci. Technol. 62, 1967–1974. https://doi.org/10.2166/wst.2010.044.

Ostace, G.S., Baeza, J.A., Guerrero, J., Guisasola, A., Cristea, V.M., Agachi, P.Ș., Lafuente, F.J., 2013. Development and economic assessment of different WWTP control strategies for optimal simultaneous removal of carbon, nitrogen and phosphorus. Comput. Chem. Eng. 53, 164–177. https://doi.org/10.1016/j.compchemeng.2013.03.007.

Otterpohl, R., Freund, M., 1992. Dynamic models for clarifiers of activated sludge plants with dry and wet weather flows. Water Sci. Technol. 26, 1391–1400. https://doi.org/10.2166/wst.1992.0582.

Pocquet, M., Wu, Z., Queinnec, I., Spérandio, M., 2016. A two pathway model for N 2 O emissions by ammonium oxidizing bacteria supported by the NO/N 2 O variation. Water Res. 88, 948–959. https://doi.org/10.1016/j.watres.2015.11.029.

Rieger, L., Alex, J., Winkler, S., Boehler, M., Thomann, M., Siegrist, H., 2003. Progress in sensor technology–progress in process control? Part 1: sensor property investigation and classification. Water Sci. Technol. 47, 103–112. https://doi.org/10.2166/wst.2003.0096.

Santín, I., Barbu, M., Pedret, C., Vilanova, R., 2018. Fuzzy logic for plant-wide control of biological wastewater treatment process including greenhouse gas emissions. ISA Trans 77, 146–166. https://doi.org/10.1016/j.isatra.2018.04.006.

Santín, I., Barbu, M., Pedret, C., Vilanova, R., 2017. Control strategies for nitrous oxide emissions reduction on wastewater treatment plants operation. Water Res. 125, 466–477. https://doi.org/10.1016/j.watres.2017.08.056.

Solís, B., Guisasola, A., Pijuan, M., Corominas, L., Baeza, J.A., 2022. Systematic calibration of N2O emissions from a full-scale WWTP including a tracer test and a global sensitivity approach. Chem. Eng. J. 134733 https://doi.org/10.1016/j.cej.2022.134733.

Solon, K., Flores-Alsina, X., Kazadi Mbamba, C., Ikumi, D., Volcke, E.I.P., Vaneeckhaute, C., Ekama, G.A., Vanrolleghem, P.A., Batstone, D.J., Gernaey, K.V., Jeppsson, U., 2017. Plant-wide modelling of phosphorus transformations in wastewater treatment systems: impacts of control and operational strategies. Water Res. 113, 97–110. https://doi.org/10.1016/j.watres.2017.02.007.

Solon, K., Flores-Alsina, X., Mbamba, C.K., Volcke, E.I.P., Tait, S., Batstone, D., Gernaey, K.V., Jeppsson, U., 2015. Effects of ionic strength and ion pairing on (plant-wide) modelling of anaerobic digestion. Water Res. 70, 235–245. https://doi.org/10.1016/j.watres.2014.11.035.

Stare, A., Vrečko, D., Hvala, N., Strmčnik, S., 2007. Comparison of control strategies for nitrogen removal in an activated sludge process in terms of operating costs: a simulation study. Water Res. 41, 2004–2014. https://doi.org/10.1016/j.watres.2007.01.029.

Stumm, W., Morgan, J.J., 1996. Aquatic Chemistry: Chemical Equilibria and Rates in Natural Waters, 3rd ed. John Wiley and Sons, New York, NY, USA.

Su, Q., Domingo-Félez, C., Zhang, Z., Blum, J.M., Jensen, M.M., Smets, B.F., 2019. The effect of pH on N2O production in intermittently-fed nitritation reactors. Water Res. 156, 223–231. https://doi.org/10.1016/j.watres.2019.03.015.

Sweetapple, C., Fu, G., Butler, D., 2015. Does carbon reduction increase sustainability? A study in wastewater treatment. Water Res. 87, 522–530. https://doi.org/10.1016/j.watres.2015.06.047.

Sweetapple, C., Fu, G., Butler, D., 2014. Multi-objective optimisation of wastewater treatment plant control to reduce greenhouse gas emissions. Water Res. 55C, 52–62. https://doi.org/10.1016/j.watres.2014.02.018.

Takács, I., Patry, G.G., Nolasco, D., 1991. A dynamic model of the clarification-thickening process. Water Res. 25, 1263–1271. https://doi.org/10.1016/0043-1354(91)90066-Y.

Torà, J.a, Lafuente, F.J., Baeza, J.A., Carrera, J., 2010. Combined effect of inorganic carbon limitation and inhibition by free ammonia and free nitrous acid on ammonia oxidizing bacteria. Bioresour. Technol. 101, 6051–6058. https://doi.org/10.1016/j.biortech.2010.03.005.

Vaneeckhaute, C., Claeys, F.H.A., Tack, F.M.G., Meers, E., Belia, E., Vanrolleghem, P.A., 2018. Development, implementation, and validation of a generic nutrient recovery model (NRM) library. Environ. Model. Softw. 99, 170–209. https://doi.org/10.1016/j.envsoft.2017.09.002.

Vanrolleghem, P.A., Corominas, L., Flores-Alsina, X., 2010. Real-Time Control and Effluent Ammonia Violations Induced by Return Liquor Overloads. Proc. Water Environ. Fed. 2010, 7101–7108. https://doi.org/10.2175/193864710798207503.

Wentzel, M.C., Ekama, G.A., Sötemann, S.W., 2006. Mass balance-based plant-wide wastewater treatment plant models - Part 1: biodegradability of wastewater organics under anaerobic conditions. Water SA 32, 269–275. https://doi.org/10.4314/wsa.v32i3.5261.

Wett, B., Rauch, W., 2003. The role of inorganic carbon limitation in biological nitrogen removal of extremely ammonia concentrated wastewater. Water Res. 37, 1100–1110. https://doi.org/10.1016/S0043-1354(02)00440-2.

Zhang, W., Wang, D., Jin, Y., 2018. Effects of inorganic carbon on the nitrous oxide emissions and microbial diversity of an anaerobic ammonia oxidation reactor. Bioresour. Technol. 250, 124–130. https://doi.org/10.1016/j.biortech.2017.11.027.